ACS Catalysis

pubs.acs.org/acscatalysis Research Article

Ligand-Controlled Regioreversed 1,2-Aryl-Aminoalkylation of Alkenes Enabled by Photoredox/Nickel Catalysis

Fu Ye,[#] Songlin Zheng,[#] Yixin Luo,[#] Xiaotian Qi,* and Weiming Yuan*

Cite This: *ACS Catal.* 2024, 14, 8505−8517 Read Online

ACCESS | Metrics & More | Article Recommendations | Supporting Information

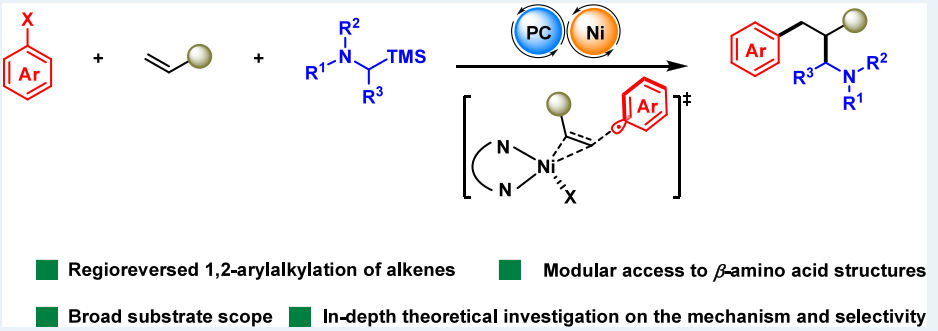

ABSTRACT: A ligand-controlled regioreversed 1,2-arylalkylation of alkenes via photoredox/nickel dual catalysis is reported. In contrast with previous reports on photoredox/nickel-catalyzed 1,2-alkylarylation reactions that initiate from the Giese addition of an alkyl radical to alkene, this three-component conjugate coupling process occurs through nickel-catalyzed aryl radical addition to alkene, thereby leading to a complementary regioselectivity to conventional 1,2-alkylarylation. An *ortho*-substituted bipyridyl ligand is the key to tune the regioselectivity, which was found to be dictated by the reactivity of alkene-coordinated $L_nNi(0)$ complexes that trigger the formation of aryl radicals via halogen-atom transfer (XAT). This regioreversed transformation allows a concise entry to structurally abundant *β*-amino acid derivatives, including ORL1-receptor antagonists.

KEYWORDS: *photoredox catalysis, nickel, radical addition to alkene, dicarbofunctionalization, β-amino acid*

INTRODUCTION

Nickel-catalyzed 1,2-dicarbofunctionalization (DCF) of alkenes represents a versatile synthetic platform for the construction of structurally diverse architectures by concomitant formation of two C−C bonds in a step- and operation-economic fashion.[1] This valuable transformation enables rapid access in molecular complexity. Classical methods involve the use of organometallic reagents via a two-electron transfer way.[2] A formidable challenge associated with this ionic pathway is the high propensity of *β*-hydride elimination from sp^3C−M intermediates, thus leading to poor compatibility of the Csp^3-hydridized coupling partners. Accordingly, significant advancement in nickel-catalyzed 1,2-DCFs based on a radical pathway has been achieved,[3] which provides a complementary approach to the ionic pathway, allows the use of Csp^3-hydridized reagents, and shows a higher level of functional group compatibility.

Recently, metallaphotoredox catalysis[4] has emerged as a powerful strategy for various bond formation events with good reactivity and novel selectivity. In this context, a variety of native Csp^3-hydridized nucleophiles can be used as alkyl radical precursors instead of highly reactive organometallic reagents in photoredox/nickel-catalyzed alkene 1,2-DCFs.[5] Despite tremendous advances in this avenue,[6] these radical relay processes are generally triggered by radical addition of alkyl radical to alkene, and the regioselectivity is directed by the radical polarity matching effect,[7] thus rendering the installation of alkyl groups at the terminal position of alkenes to deliver *1,2-alkylarylation* products exclusively (Scheme 1a, left). By contrast, 1,2-DCF initiated by 1,2-migratory insertion of an aryl-M species across the C=C bond (Heck-type reaction) followed by coupling with an alkyl radical at the internal olefinic position would afford regioreversed *1,2-arylalkylation* products (Scheme 1a, right). However, this complementary reactivity has yet to be developed, presumably due to the very fast rate of radical addition of alkyl radicals to electron-deficient alkenes.[8] Moreover, the regioreversed transformation may compete with side reactions, including two-component cross-coupling, (reductive) Heck reaction, traditional Giese addition, and reductive dehalogenation. Our

Received: March 1, 2024
Revised: May 8, 2024
Accepted: May 8, 2024
Published: May 16, 2024

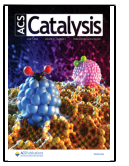

https://doi.org/10.1021/acscatal.4c01312
ACS Catal. 2024, 14, 8505−8517

Scheme 1. State of the Art of Photoredox/Nickel Dual-Catalyzed 1,2-Dicarbofunctionalization of Alkenes

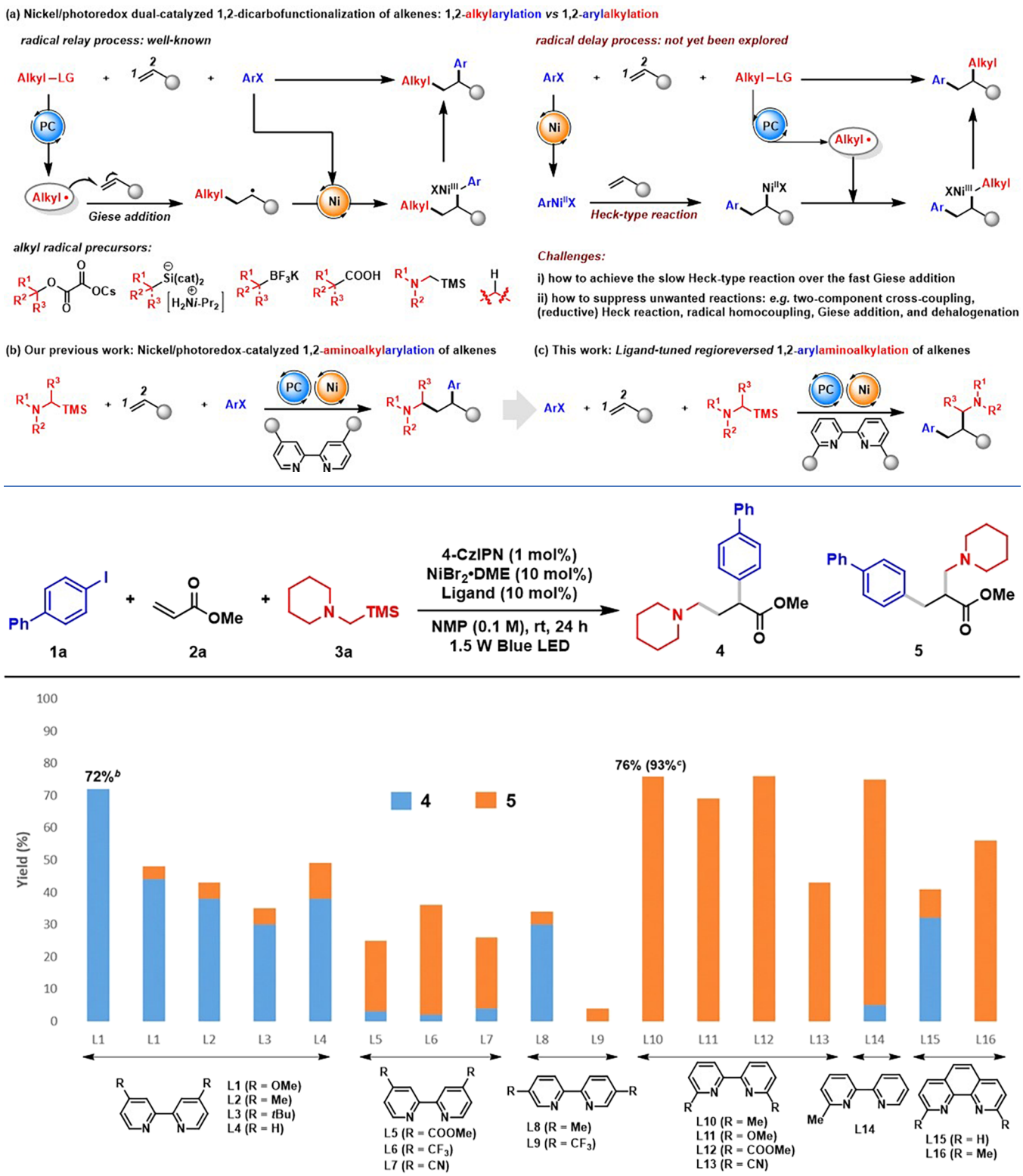

Figure 1. Condition optimization for ligand-controlled regioreversed 1,2-arylaminoalkylation of alkenes. [a]All reactions were carried out on a 0.1 mmol scale, **1a**/**2a**/**3a** = 1:2:2 (molar ratio), corrected GC yields using *n*-tridecane as the internal standard. [b]DMF as solvent. [c]4-CzIPN (0.5 mol %), NMP (0.2 M), **1a**/**2a**/**3a** = 1.5:1:1.5.

group has recently reported a three-component conjugate cross-coupling of α-silylamines, electron-deficient alkenes, and aryl halides via a dual photoredox/nickel catalysis (Scheme 1b).[9] We proposed that the radical relay process was initiated by Giese addition of α-amino radicals to alkenes followed by a sequent single-electron transmetalation, oxidative addition of aryl halides, and reductive elimination (cf. Scheme 1a, left) to afford 1,2-aminoalkylarylation products with good efficiency

https://doi.org/10.1021/acscatal.4c01312
ACS Catal. 2024, 14, 8505−8517

Scheme 2. Substrate Scope for Photoredox/Nickel-Catalyzed Regioreversed 1,2-Arylaminoalkylation of Alkenes[a]

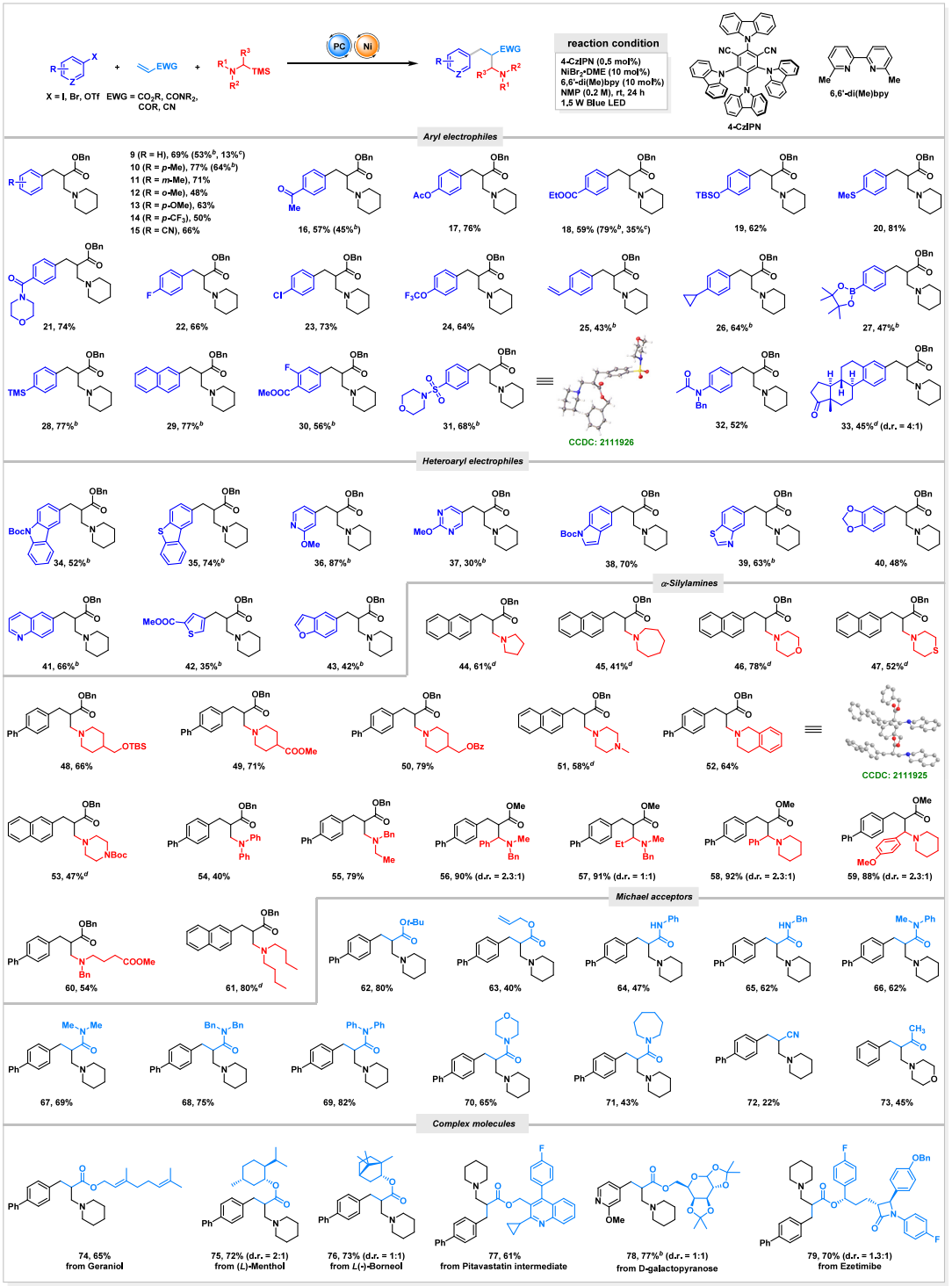

[a]Unless otherwise noted, all reactions were carried out on a 0.3 mmol scale with aryl iodide (0.45 mmol, 1.5 equiv), alkene (0.3 mmol, 1.0 equiv), and α-silylamine (0.45 mmol, 1.5 equiv). Isolated yields after chromatography are shown. [b]Aryl bromide was used. [c]Aryl chloride used. [d]Aryl triflate was used.

and regioselectivity. Based on the previous work[5,9] and our ongoing interest in alkene 1,2-difunctionalizations,[10] we questioned whether it would be possible to reverse the regioselectivity via steering Heck-type addition of aryl electrophiles to alkenes as the initiation step to trigger the tandem process instead of the Giese addition of alkyl radicals to alkenes. If possible, it would allow regiodivergent synthesis[11] of structurally diverse molecules from the same starting materials. Herein, we report the successful realization of such a 1,2-DCF with complementary regioselectivity simply by tuning the ligand (Scheme 1c). It is very interesting to find that *ortho*-substituted bipyridyl ligands can reverse the regioselectivity to afford 1,2-arylaminoalkylation products exclusively. Such a "radical delay" process provides an efficient and

https://doi.org/10.1021/acscatal.4c01312
ACS Catal. 2024, 14, 8505−8517

modular synthetic platform for a variety of highly valuable β^2 and $\beta^{2,3}$-amino acid structures. In addition, we performed a series of mechanistic studies including quantum mechanical calculations to gain deep insight into the mechanism and the origin of the reversed selectivity.

RESULTS AND DISCUSSION

Recently, we reported a three-component conjugate cross-coupling reaction of α-silylamines, electron-deficient alkenes, and aryl halides via a dual photoredox/nickel catalysis.[9] This radical relay process affords 1,2-aminoalkylarylation product **4** exclusively, where an α-aminoalkyl fragment was added into the terminal position of alkenes, whereas an aryl group was added into the internal position, by applying 4,4′-di(OMe)bpy (**L1**) as ligand in DMF. To our surprise, when changing the solvent to NMP, we could detect a trace amount of a new product (4% GC yield), whose structure was determined as the regioreversed product **5**. The molar ratio of the two regioisomers (rr) is 11/1. Apart from these two regioisomers, several competitive side products arising from two-component cross-coupling (**6**), Giese addition (**7**), and reductive Heck reaction (**8**) were detected (not shown; see the Supporting Information for details). This preliminary result inspired us to perform a detailed survey of various electronically and sterically varying bipyridyl (bpy) ligands (Figure 1). Other bpy ligands bearing electron-rich *para* substituents such as Me (**L2**) or *t*Bu (**L3**) provided similar results. The parental bpy (**L4**) could slightly increase the ratio of the regioreversed product (rr = 4/1). Interestingly, ligands containing electron-deficient substituents such as CO_2Me (**L5**), CF_3 (**L6**), or CN (**L7**) resulted in a reversed regioselectivity and afforded product **5** predominantly, albeit in a totally low yield. *Meta*-Me-substituted bpy (**L8**) gave a comparable selectivity to the *para*-Me-substituted variant (**L2**). However, installing electron-deficient substituents on the *meta* position is inferior to the reaction (**L9**). To our delight, when using *ortho*-substituted bpy ligands, irrespective of the electronic nature of the ligands (**L10**, **L11**, **L12**, and **L13**), all reactions afforded the regioreversed product **5** exclusively with very good yields. Of note, *ortho* monosubstituted bpy ligand (**L14**) is enough to achieve a satisfactory regioreversion (rr = 1/14) and reactivity. A similar trend was observed when using 1,10-phenanthroline type ligands (**L15** vs **L16**). Thus, we chose 6,6′-di(Me)bpy (**L10**) as the optimal ligand to further investigate other reaction parameters (see the Supporting Information for details). Finally, we could afford 93% GC yield (87% isolated yield) when adjusting the molar ratio of **1a**/**2a**/**3a** to 1.5:1:1.5 and increasing the concentration to 0.2 M. Under this condition, the catalytic loading of the organic photocatalyst (4-CzIPN) can be further decreased to as low as 0.5 mol %. Other silyl substituents such as $SiMe_2Ph$ were examined with a lower reactivity (64% GC yield, not shown). Control experiments revealed that nickel, the photocatalyst, and visible light irradiation are all indispensable for the reaction. Of note, the reaction could still afford 37% yield of **5** with a good regioreversion (rr = 1/19) in the absence of the ligand, indicating that NMP may serve as a ligand as *ortho*-substituted bpy to guarantee an excellent regioreversion (see Figure S49 for DFT studies).

With the optimized reaction conditions in hand, the substrate scope of the regioreversed 1,2-arylaminoalkylation was investigated (Scheme 2). The electronic and steric environments of aryl halides have no significant influence on the reactivity (**9**−**33**). A variety of functional groups, including trifluoromethyl, cyano, ketone, acetoxyl, ester, OTBS, thioether, amide, fluoro, chloro, trifluoromethoxyl, alkene, cyclopropane, boronic ester, silyl, and sulfamide, are well tolerated to give the corresponding β-aminoesters in good yields (**14**−**32**). Aryl triflate derived from the naturally occurring product estrone was also compatible (**33**). Particularly noteworthy was the tolerance of reaction conditions to the boron, halogen, silyl, and alkene functionalities, which provide a versatile synthetic platform for further elaboration. Aryl bromides display a comparable reactivity (**9**, **10**, **16**, **18**, **25**−**31**). Even aryl chlorides can also be tolerated, and the yield can be increased by installing an electron-deficient group (**9** vs **18**). Moreover, a variety of heteroaromatic rings, which are common scaffolds in the preparation of medicinally relevant molecules, such as carbazole, benzo[*b*,*d*]thiophene, pyridine, pyrimidine, indole, benzo[*d*]thiazole, benzo[*d*][1,3]dioxole, quinoline, thiophene and benzofuran, are incorporated smoothly (**34**−**43**). Under the standard conditions, aryl bromides, aryl iodides, and aryl triflates are all potent substrates to engage the conjugate coupling process, showcasing the exceptional functional group compatibility and broad applicability for aryl electrophiles of the method.

Next, we turned our attention to evaluating the scope generality of α-silylamines and alkenes. Given the importance of heterocyclic amine architectures in pharmaceutical chemistry, facile introduction of these moieties into target compounds is of great interest. Our method provides a straightforward approach to incorporate various heterocyclic amine moieties including pyrrolidine, piperidine, azepane, morpholine, thiomorpholine, piperazine, and tetrahydroisoquinoline (**44**−**53**) to synthesize structurally diverse β-amino acid derivatives in good yields. Both symmetrical and unsymmetrical acyclic α-silylamines coupled as well (**54**−**61**). Of particularly note, α-aryl or alkyl-branched silylamines reacted smoothly and furnished the desired products with two adjacent tertiary carbon centers (**56**−**59**). Besides methyl and benzyl acrylates, allyl and sterically bulky *t*-Bu-substituted acrylates proceeded as well (**62**, **63**). Moreover, both acyclic and cyclic acrylamides even with a free NH group reacted smoothly to afford β-amino amides in good yields (**64**−**71**). Finally, the Michael acceptors can be further extended to enones and acrylonitriles (**72**, **73**). Unfortunately, the use of α or β-branched alkenes is currently a limitation in this reaction. To further demonstrate the synthetic potential of our developed methodology, a diverse range of structurally complex alkenes derived from natural products and drug-like molecules (geraniol, *L*(−)-menthol, *L*(−)-borneol, D-galactopyranose, pitavastatin, and ezetimibe) were examined. To our delight, the existing sensitive functionalities and structural complexity exert a negligible influence on the efficiency, leading to potentially valuable products with good yields (**74**−**79**). The structures of the products were confirmed unambiguously by X-ray diffraction analysis of products **31** and **52**.

In addition, we were delighted to find that the current regioreversed 1,2-arylaminoalkylation can be further extended to alkenyl electrophiles (Scheme 3). Only a slight change in the ligand (**L10** to **L12**) and photocatalyst (4-CzIPN to $Ir(ppy)_2(dtbbpy)PF_6$) was required with the aim to increase the yield. As vinyl triflates are more easily accessible than the corresponding vinyl halides from ketones by a single-step operation, a series of vinyl triflates were synthesized and subjected to the modified conditions. Pleasingly, cyclic vinyl

https://doi.org/10.1021/acscatal.4c01312
ACS Catal. 2024, 14, 8505−8517

Scheme 3. Substrate Scope of Vinyl Electrophiles[a]

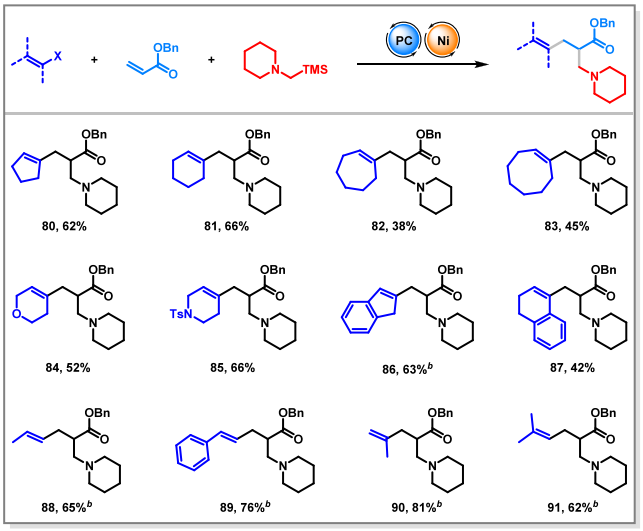

[a]Unless otherwise noted, all reactions were carried out on a 0.3 mmol scale with $Ir(ppy)_2(dtbbpy)PF_6$ (0.5 mol %), $NiBr_2$·DME (10 mol %), 6,6′-di(COOMe)bpy (10 mol %), vinyl triflate (0.45 mmol, 1.5 equiv), alkene (0.3 mmol, 1.0 equiv), and α-silylamine (0.45 mmol, 1.5 equiv) in NMP (0.2 M) at rt for 24 h under 1.5 W blue LED irradiation. Isolated yields after chromatography are shown. [b]Aryl bromide was used.

triflates ranging from five- to eight-membered rings were coupled smoothly to give the target products in good yields (**80**−**83**). Heterocyclic vinyl triflates and benzene-fused substrates were also tolerated (**84**−**87**). Moreover, a series of acyclic vinyl triflates containing α-substituent, β-substituent, and β,β-disubstituents were incorporated smoothly to provide structurally diverse β-amino acid backbones with an extra alkene functionality, a synthetic versatile group for further derivations (**88**−**91**).

The reaction could be scaled up to a 3 mmol scale without an obvious decrease in yield (Scheme 4a). β-Amino acid scaffolds widely exist in biologically active compounds.[12] To further demonstrate the synthetic potential of the present method in more structurally complex contexts, applications of this protocol for the concise synthesis of pharmaceutically relevant molecules were investigated (Scheme 4b). ORL1 (opioid receptor-like 1) antagonists are useful for treating various CNS (central nervous system) diseases and contain a unit of β-amino acid structure.[13] The literature method[13] toward their synthesis requires four steps including *aza*-Michael addition, alkylation, hydrolysis, and condensation. Because of the low efficiency of *aza*-Michael addition and alkylation, the overall yield was very low (<15%). Gratifyingly, we can furnish the synthesis with a two-step manipulation involving an S_N2 reaction and the regioreversed 1,2-arylaminoalkylation, thus enabling a fast and divergent access to ORL1-receptor antagonists in much higher yields from the same starting material spiropiperidine (**92**−**96**). Our synthetic procedure could obviate the handle of harsh conditions (e.g., strong bases, acids, or extreme negative temperatures).

MECHANISTIC STUDIES

We are very curious about the dichotomy between our previous work[9] and the reversed regioselectivity presented here, where exactly the same reaction takes place but with

Scheme 4. Gram-Scale Reaction and Synthetic Applications

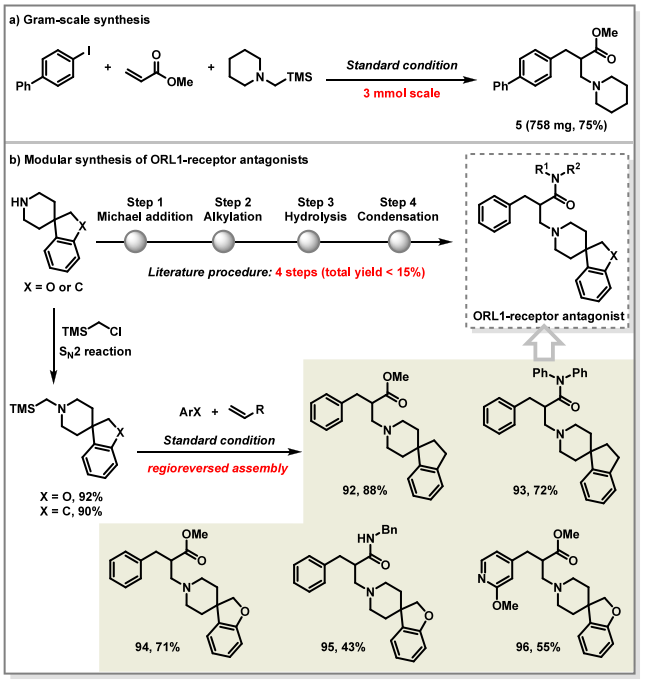

opposite regioselectivity. It seems that the ligand plays a critical role in determining the regioisomer distribution. To investigate the coupling mechanism and clarify the ligand effects on regioselectivity control, density functional theory (DFT) calculations were carried out. According to the experimental conditions, Ni(0) species can be generated in situ by photocatalytic single electron reduction of the Ni(II) precatalyst[9,10a] and is thus used in the calculation of free energy profiles. DFT studies suggest that the most stable Ni(0) species contains the coordination of one bidentate ligand and one alkene (this affinity was reflected by a UV−vis absorption experiment; see Figures S14 and S15). As shown in Figure 2, the free energy profile of Ni(0)/**L1**-catalyzed 1,2-amino-alkylarylation starts from singlet Ni(0) complex **97**, α-amino radical **98**, alkene **2a**, and iodobenzene **1b**. For the transformation of α-amino radical **98**, both the reactions with the Ni(0) complex and alkene are considered (Figure 2a). Although the radical addition to the Ni(0) center via transition state **TS-1** has a lower energy barrier ($\Delta G^{\ddagger}$ = 4.0 kcal/mol), the generated Ni(I) complex **99** cannot be transformed to the product due to the higher activation free energy of migratory alkene insertion ($\Delta G^{\ddagger}$ = 22.9 kcal/mol, see Figure S38 for details). The interplay between α-amino radical **98** and Ni(0) complex **97** can be regarded as radical buffering, which denotes the off-cycle equilibrium. The radical dissociation will occur through homolytic C−Ni(I) bond cleavage in **99** to release α-amino radical **98**, which then undergoes Giese addition (via **TS-2**) to form the more stable α-carbonyl radical **100**. The energy barrier with respect to Ni(I) complex **99** is 16.4 kcal/mol. It should be noted that the Giese addition is irreversible because the formation of **100** is exergonic by 12.2 kcal/mol and the following radical addition of **100** to the Ni(0) center of **97** via **TS-3** only requires an energy barrier of 3.3 kcal/mol. The formation of the γ-amino Ni(I) complex **101** is also highly exergonic. Subsequently, alkene **2a** may dissociate from **101**, and the concerted oxidative addition of iodobenzene **1b** to Ni(I) complex **102** ($\Delta G^{\ddagger}$ = 16.4 kcal/mol) followed by the

https://doi.org/10.1021/acscatal.4c01312
ACS Catal. 2024, 14, 8505−8517

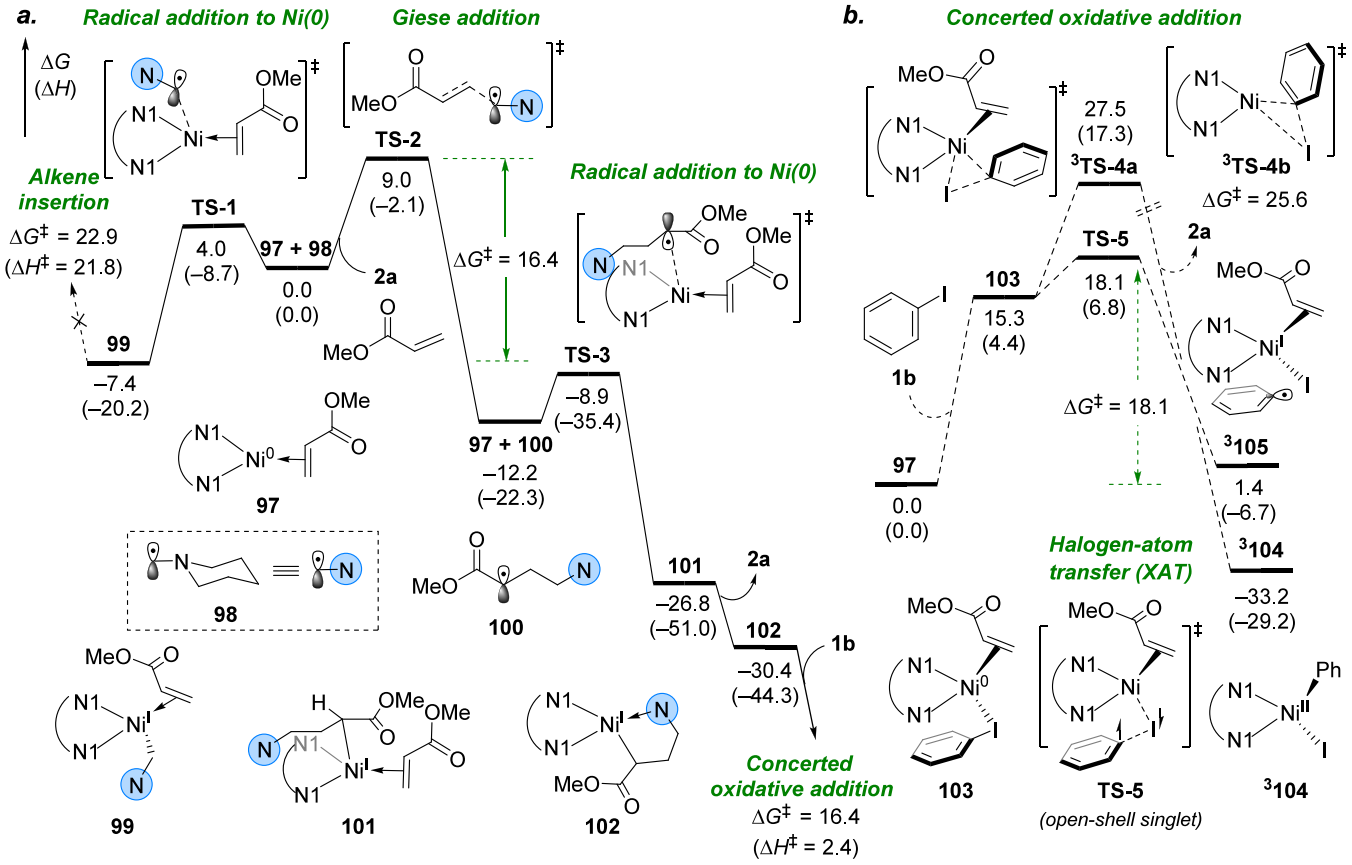

Figure 2. Computational study of Ni(0)/**L1**-catalyzed 1,2-aminoalkylarylation. The bidentate ligand used in the DFT calculation is 4,4′-di(OMe)bpy (**L1**). (a) Free energy profile of the favored reaction pathway initiates from Giese addition and radical addition to Ni(0). (b) Free energy profile of the reaction between iodobenzene and Ni(0) complex **97**. All energies were calculated at the ωB97XD/6-311+G(d,p)−LANL08(f) (for Ni)−(LANL08(d)(for I)/SMD(DMF)//B3LYP-D3(BJ)/6-31G(d)−LANL2DZ (for Ni)−LANL2DZdp (for I) level of theory. The energies are given in kcal/mol. See SI for full free energy profiles, including the alkene insertion step and concerted oxidative addition of **1b** to complex **102** (Figures S38−S42).

C−C reductive elimination from the phenyl Ni(III) complex ($\Delta G^{\ddagger}$ = 7.3 kcal/mol) affords the 1,2-aminoalkylarylation product (see Figure S39 for details).

Besides α-amino radical **98**, the direct reaction of iodobenzene **1b** with Ni(0) complex **97** is also studied. As shown in Figure 2b, the corresponding concerted oxidative addition transition states leading to the formation of triplet aryl Ni(II) complex ^{3}**104** are located as ^{3}**TS-4a** and ^{3}**TS-4b**. The activation free energy of ^{3}**TS-4a** is 27.5 kcal/mol. We surmise that the higher energy barrier can be attributed to the great distortion of the alkene moiety. Because of the d to π* backdonation in the planar structure of **97**, alkene **2a** is tightly bound to the Ni(0) center.[14] Meanwhile, the concerted oxidative addition of **1b** to the Ni(0) center forces the alkene moiety to distort from the coordination plane to construct the tetrahedral configuration shown in ^{3}**TS-4a**, and the interaction of iodobenzene with Ni(0) is insufficient to compensate the distortion penalty, thereby resulting in the higher energy barrier. The dissociation of alkene is also disfavored for a similar reason. The corresponding transition state without the coordination of an alkene, ^{3}**TS-4b**, has a high activation free energy of 25.6 kcal/mol.

In addition to the concerted oxidative addition mechanism, we also considered a Ni(0)-mediated halogen-atom transfer (XAT) mechanism[15] for C−I bond activation. As shown in Figure 2b, an open-shell singlet XAT transition state is located as **TS-5**. The activation free energy is 18.1 kcal/mol, which is still higher than that shown in Figure 2a. Thus, this XAT mechanism can also be ruled out for the Ni(0)/**L1**-catalyzed 1,2-aminoalkylarylation process. However, the Ni(0)/**L10**-mediated XAT mechanism is found to be viable for the 1,2-arylaminoalkylation process. As shown in Figure 3a, the iodine atom of iodobenzene **1b** can approach the Ni(0) center from beneath the coordination plane of Ni(0) complex **106** and forms tetrahedral Ni(0) complex **107**. Through XAT transition state **TS-6**, homolytic C−I bond cleavage occurs with an activation free energy of 13.0 kcal/mol to generate triplet intermediate ^{3}**108**. The phenyl radical moiety in ^{3}**108** can easily dissociate and then attack the terminal carbon of the alkene that coordinated to the Ni(0) center through transition state ^{3}**TS-7** ($\Delta G^{\ddagger}$ = 5.6 kcal/mol). This metal-alkene coupled radical addition occurs on a triplet free energy profile, as the spin states of the transition state and the generated alkyl Ni(II) complex ^{3}**111** are all triplet. It is noteworthy that this radical addition outcompetes the phenyl radical addition to the Ni(I) center through ^{3}**TS-9** ($\Delta G^{\ddagger}$ = 9.8 kcal/mol). The higher energy barrier of ^{3}**TS-9** can be ascribed to the tetrahedral configuration of Ni(I) complex **109** that hinders the approach of the phenyl radical to the metal center. Moreover, the smaller steric hindrance above the alkene moiety in **109** and the high reactivity of phenyl radical[16] jointly result in the lower energy barrier of metal-alkene coupled radical addition transition state

https://doi.org/10.1021/acscatal.4c01312
ACS Catal. 2024, 14, 8505−8517

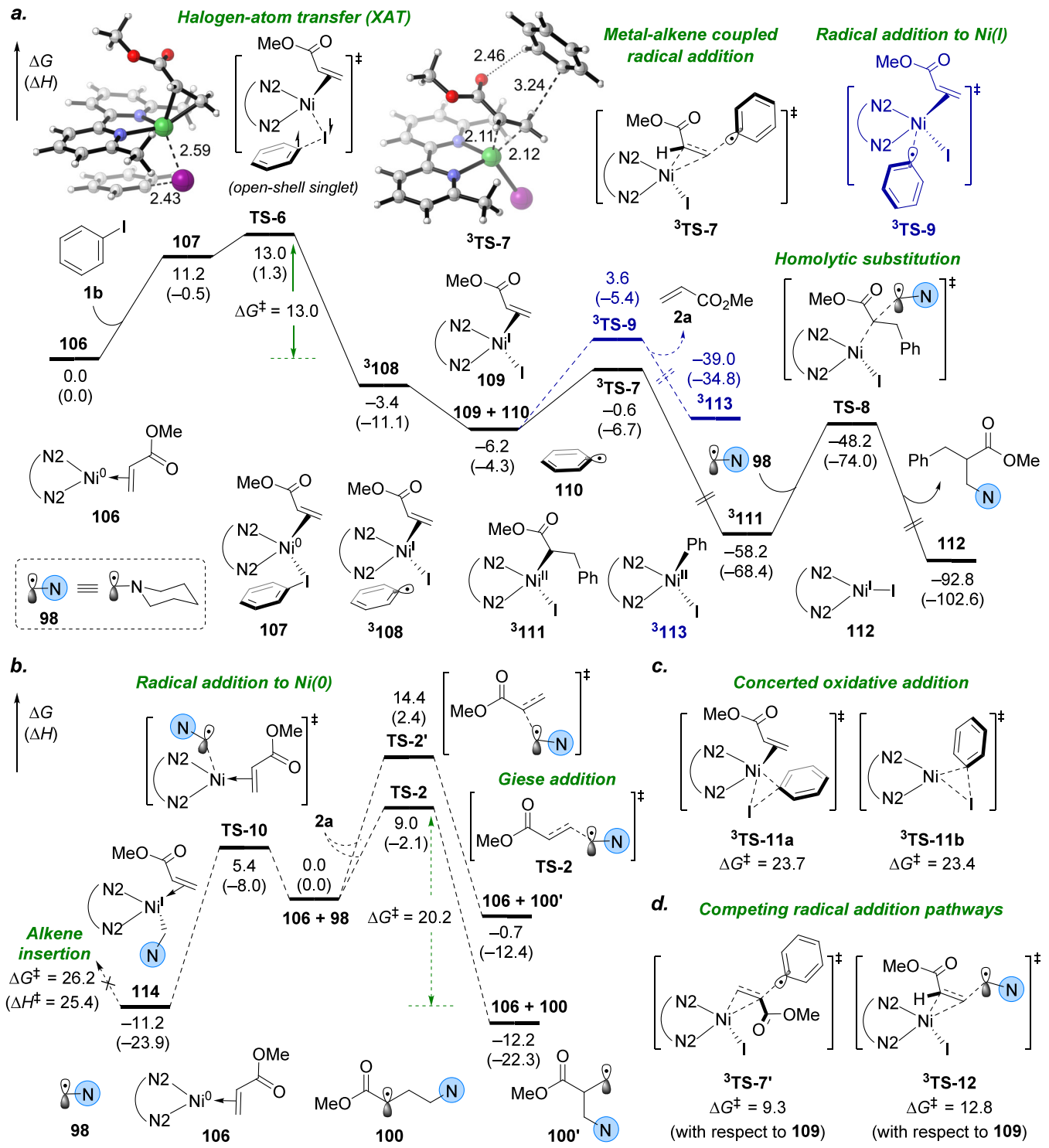

Figure 3. Computational study of Ni(0)/**L10**-catalyzed 1,2-arylaminoalkylation. The bidentate ligand used in the DFT calculation is 6,6′-di(Me)bpy (**L10**). (a) Free energy profile of the favored reaction pathway that initiates from the halogen atom transfer (XAT) and metal-alkene coupled radical addition. (b) Free energy profile of regioselective Giese addition and radical addition to Ni(0)/**L10**. (c) Concerted oxidative addition of iodobenzene to Ni(0) complex **106** through cyclic transition states. (d) Competing metal-alkene coupled radical addition with phenyl radical and α-amino radical for the discussion of the regioselectivity control. All energies were calculated at ωB97XD/6-311+G(d,p)−LANL08(f) (for Ni)−(LANL08(d) (for I)/SMD(DMF)//B3LYP-D3(BJ)/6-31G(d)−LANL2DZ (for Ni)−LANL2DZdp (for I) level of theory. The energies are in kcal/mol. See SI for full free energy profiles (Figures S43−S47).

^{3}**TS-7**. Therefore, alkyl Ni(II) complex ^{3}**111**, instead of aryl Ni(II) complex ^{3}**113**, is formed in this case.

Finally, the 1,2-arylaminoalkylation product is generated through the α-amino radical **98** triggered homolytic substitution transition state **TS-8** ($\Delta G^{\ddagger}$ = 10.0 kcal/mol, Figure 3a). The competing pathway for C−C bond formation that consists of the α-amino radical addition to ^{3}**111** followed by C−C reductive elimination from Ni(III) is supposed to be less

https://doi.org/10.1021/acscatal.4c01312
ACS Catal. 2024, 14, 8505−8517

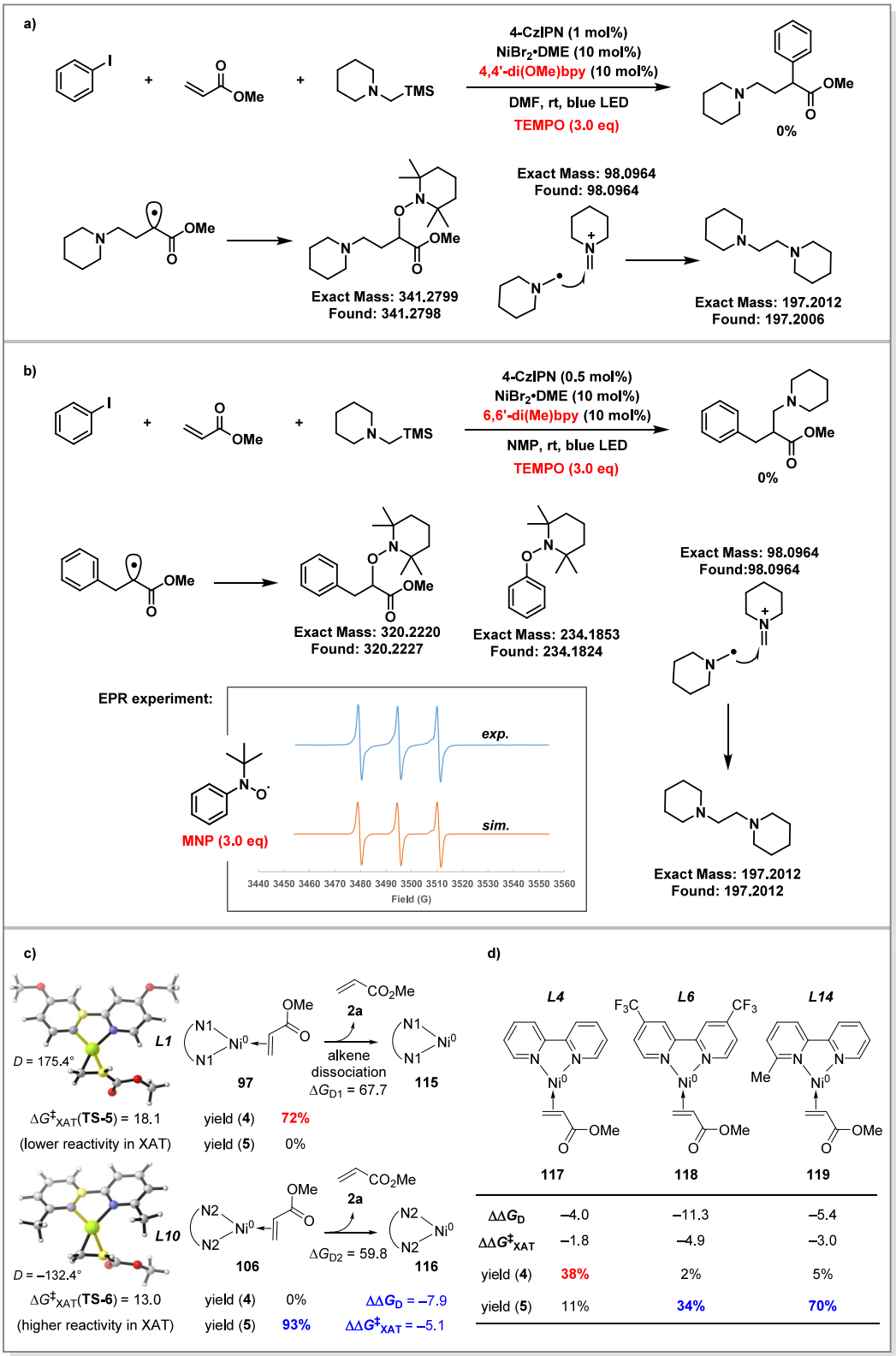

Figure 4. Mechanistic studies. (a) Radical-probing experiments with the Ni/**L1** catalytic system. (b) Radical-probing experiments with Ni/**L10** catalytic system. (c) Probing the relationship of the alkene dissociation energy with the XAT energy barriers and the regioselectivity. $\Delta\Delta G_D = \Delta G_{D2} - \Delta G_{D1}$ and $\Delta\Delta G^{\ddagger}_{XAT} = \Delta G^{\ddagger}_{XAT}$(**TS-6**) − $\Delta G^{\ddagger}_{XAT}$(**TS-5**). (d) Validation of the ligand effects by investigating other bpy ligands (**L4**, **L6**, and **L14**) involved in XAT. All energies are in kcal/mol. $\Delta\Delta G_D$ and $\Delta\Delta G^{\ddagger}_{XAT}$ are with respect to the corresponding values of complex **97**. All of the yields are extracted from Figure 1.

likely as the tetrahedral configuration of ^{3}**111** prevents the radical addition to the metal center (see Figure S43 for details).[17] Furthermore, the Giese addition pathway with *α*-amino radical **98** can also be ruled out in the reaction using

https://doi.org/10.1021/acscatal.4c01312
ACS Catal. 2024, 14, 8505−8517

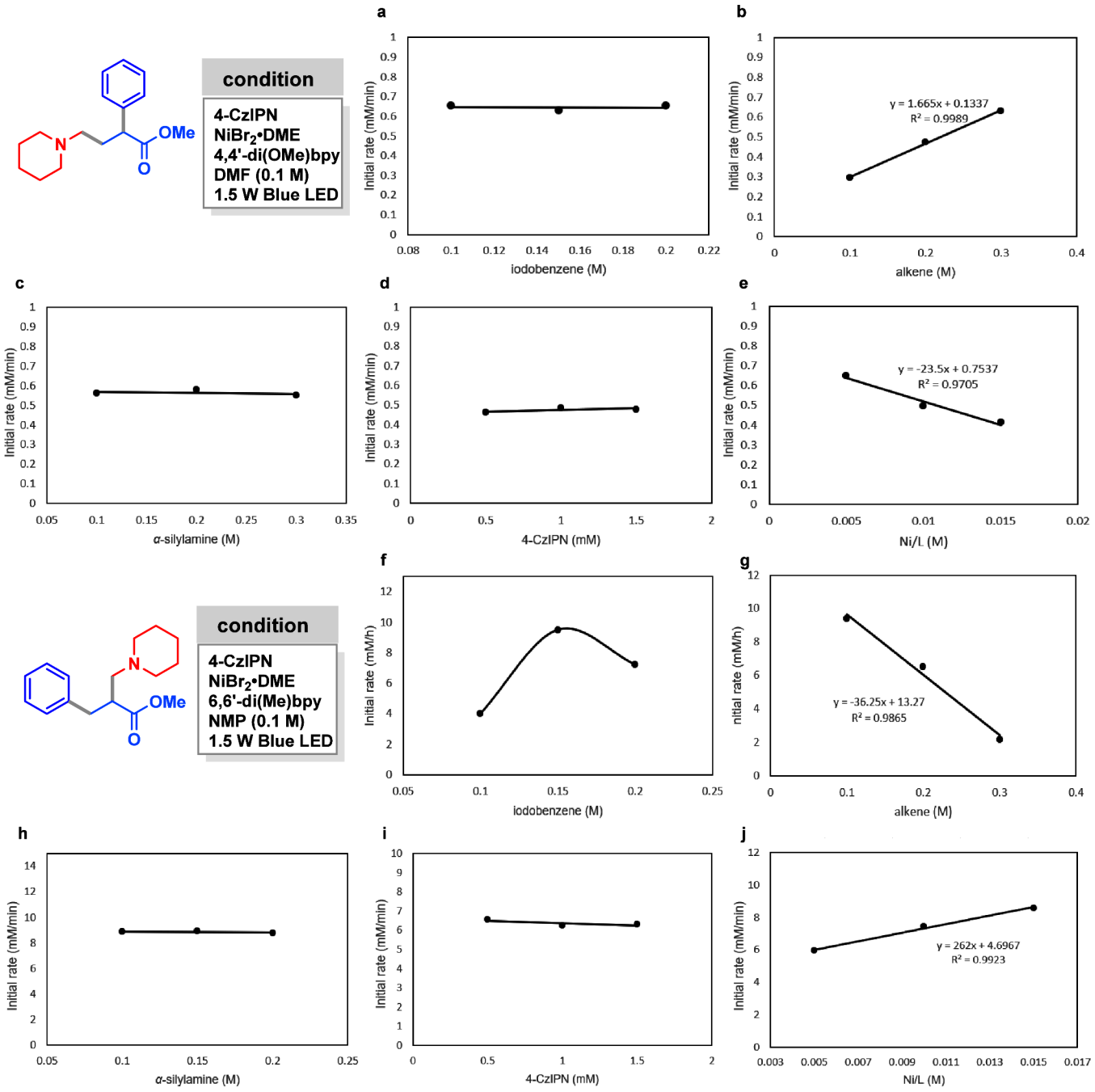

Figure 5. Kinetic studies. For Ni/**L1**-catalyzed 1,2-aminoalkylarylation: (a) plot of k_{in} versus iodobenzene concentrations. (b) plot of k_{in} versus alkene concentrations; (c) plot of k_{in} versus α-silylamine concentrations; (d) plot of k_{in} versus 4-CzIPN concentrations; and (e) plot of k_{in} versus Ni/**L1** concentrations. For Ni/**L10**-catalyzed 1,2-arylaminoalkylation: (f) plot of k_{in} versus iodobenzene concentrations; (g) plot of kin versus alkene concentrations; (h) plot of k_{in} versus α-silylamine concentrations; (i) plot of k_{in} versus 4-CzIPN concentrations; and (j) plot of k_{in} versus Ni/**L10** concentrations.

6,6′-di(Me)bpy (**L10**). As shown in Figure 3b, the energy barrier of **TS-2** with respect to Ni(I) complex **114** is 20.2 kcal/mol. Considering that the concentration of aryl iodide is much higher than that of α-amino radical **98** and the energy barrier of XAT is lower in the case with **L10** ($\Delta G^{\ddagger}$ = 13.0 kcal/mol), Ni(0) complex **106** will preferentially react with the aryl iodide through **TS-6** to accomplish the XAT process (Figure 3a).

The regioselectivity of alkene 1,2-dicarbofunctionalization is also investigated. First, the Markovnikov addition of α-amino radical **98** to alkene through **TS-2′** is disfavored (Figure 3b). Second, the Heck-type mechanism that involves the concerted oxidative addition of aryl iodide to Ni(0) followed by migratory insertion of alkene into the Ni−C(sp^2) bond is also studied as the phenyl group will be added to the terminal carbon of alkene. However, the higher activation free energies of concerted oxidative addition transition states ^{3}**TS-11a** and ^{3}**TS-11b** (Figure 3c) indicate that this mechanism is disfavored for this reaction (see Figure S45 for details). Finally, the competing metal-alkene coupled radical addition pathway with phenyl radical attacks the internal carbon of alkene (via ^{3}**TS-7′**), and α-amino radical attacks the terminal carbon of alkene (via ^{3}**TS-12**), which are also ruled out because of the higher

https://doi.org/10.1021/acscatal.4c01312
ACS Catal. 2024, 14, 8505−8517

energy barriers. The lower reactivity of α-amino radical **98** in ^{3}**TS-12** originates from the higher stability compared to that of the phenyl radical (see Figure S47b for details).

To verify the existence of the phenyl radical and α-amino radical species, a series of radical-trapping experiments were conducted. In the Ni/**L1** catalytic system (as shown in Figure 4a), the reaction was inhibited by adding TEMPO as a radical scavenger. Instead, the α-carbonyl radical-trapped TEMPO-adduct was detected by high-resolution mass spectrometric (HRMS) analysis, which was suggested to be generated via Giese addition of α-amino radical to alkene, thus indicating the generation of α-amino radical in the system. Besides, we also detected the iminium ion species and diamine product (which was probably formed by the radical addition of α-amino radical to iminium ion intermediate[10a,18]). Although we cannot detect α-amino radical directly, probably due to its low concentration and high stability, nevertheless, all results together support the formation of α-amino radical in the Ni/**L1** catalytic system. However, under this condition, we could not collect any evidence to support the existence of aryl radical species. However, in the Ni/**L10** catalytic system (Figure 4b), an aryl radical and a structurally different α-carbonyl radical generated by aryl radical addition to alkene were trapped by TEMPO and detected by HRMS, suggesting the existence of an aryl radical. Moreover, the electron paramagnetic resonance (EPR) experiment with 2-methyl-2-nitrosopropane dimer (MNP) as a radical scavenger was further carried out. It provided a signal that was consistent with that of the aryl radical, which further confirms the formation of aryl radical in the Ni/**L10** catalytic system. These informative experiments are in accordance with the computationally proposed mechanism that aryl radical may dissociate from the solvent cage after XAT (Figure 3a) and then attack the free alkene (see Figure S47 for details). In addition, we could also detect iminium ion species and diamine product, suggesting that both the aryl radical and α-amino radical are involved in the Ni/**L10** catalytic system. The Stern−Volmer studies suggested that α-silylamine is the most efficient quencher to quench the luminescence of the excited state of photocatalyst under both catalytic systems (see Figures S2−S11). Light on/off experiments showed that both reactions require persistent irradiation (see Figures S12 and S13). Finally, UV−vis absorption experiments showed that mixing Ni(cod)$_2$, **L1** or **L10**, and alkene resulted in a significant bathochromic shift together with a new absorption peak from UV−vis absorption spectroscopy, indicating a strong interaction of nickel (0) with the bidentate ligand and alkene (see Figures S14 and S15).

To detangle the ligand effects, a thorough comparison between the computational results of **L1** and **L10** that participated in three-component coupling was performed. It suggests that the ligand effects on regioselectivity control are dominated by the reactivity of alkene-coordinated Ni(0)/Ln complexes in the XAT process. Higher reactivity in XAT enables a higher formation rate of phenyl radical and thus accelerates the metal-coupled radical addition to trigger the 1,2-arylaminoalkylation process. DFT studies reveal that this reactivity is negatively correlated with the alkene dissociation energy. As shown in Figure 4c, **L10** involved Ni(0) complex **106** has a smaller alkene dissociation energy than that of **L1**-coordinated Ni(0) complex **97** ($\Delta\Delta G_D$ = −7.9 kcal/mol), and the corresponding activation free energy of XAT is also lower ($\Delta\Delta G^{\ddagger}_{XAT}$ = −5.1 kcal/mol), which favors the 1,2-arylaminoalkylation process. Structural analysis shows that the methyl substituents of **L10** hinder the tight coordination of alkene to Ni(0) as witnessed by the smaller dihedral angle (−132.4°), which renders the configuration change and structural distortion easier amid the XAT process. In contrast, the electron-donating substituents (−OMe) of **L1** enable a tight coordination of alkene to Ni(0) due to the stronger d to π* backdonation,[14a,19] which disfavors the configuration change for XAT. The conclusion of ligand effects can also be extended to other bpy ligands (**L4**, **L6**, and **L14**) involved in XAT (Figure 4d). Notably, replacing the electron-donating substituents at the *para* site of nitrogen in **L1** with −H or electron-withdrawing group (−CF$_3$), which will weaken the backdonation, can slow down the 1,2-aminoalkylarylation process and even reverse the regioselectivity. Removing one methyl substituent from **L10** (i.e., using **L14** as the ligand) also leads to the decreased ratio of 1,2-arylaminoalkylation product due to the released steric clash with alkene. The combined experimental and computational studies validate that both the electronic and steric effects of the ligands are critical for the regioselectivity control in this reaction system.

Finally, kinetic studies were carried out under both conditions (see Figure 1, with **L1** or **L10** as the ligand) to shed light on the roles of each component (aryl halide, alkene, α-silylamine, photocatalyst, and Ni/Ln) at the rate-determining step (RDS). The molar concentrations of products **97** and **98** were plotted against the reaction time to obtain a typical reaction kinetic profile. In the Ni/**L1** catalytic system (toward 1,2-aminoalkylarylation), the kinetic studies showed that the Giese addition initiated radical relay process exhibits a first-order rate dependence on alkene (Figure 5b) but no appreciable deviation of the initial rates (k_{in}) by changing the concentration of iodobenzene (Figure 5a), α-silylamine (Figure 5c), and 4-CzIPN (Figure 5d), suggesting that the reaction is zero order on aryl iodide, α-silylamine, and the photocatalyst. However, an apparent inverse rate dependence on Ni/**L1** (Figure 5e) was observed. The increased concentration of nickel catalyst interferes with the reaction rate by the combination of Ni with alkene and α-amino radical, which diminishes the Giese addition rate of the α-amino radical to alkene. The above results suggested that the Giese addition of the α-amino radical to the alkene might be the rate-determining step. Interestingly, the kinetic profile is obviously different for 1,2-arylaminoalkylation with the Ni/**L10** catalytic system. The observed positive reliance of reaction rate upon the concentrations of the aryl iodide and nickel catalyst suggested that the nickel-mediated halogen atom abstraction of aryl iodide might be rate-determining (Figure 5f,j). However, an inverse rate dependence on aryl iodide at higher loadings was observed, probably as a result of the competitive concerted oxidative addition of aryl iodide to Ni(0) that suppresses the Ni(0)-mediated XAT pathway (Figure 3c). Similarly, no appreciable deviation in rate was observed by changing the concentration of 4-CzIPN and α-silylamine (Figure 5h,i). Meanwhile, a negative rate dependence upon the concentrations of the alkene could be rationalized by multiple ligation to the Ni(0)-catalyst, which depletes coordination sites for the incoming aryl halides to undergo inner-sphere halogen atom abstraction (Figure 5g).[3c] The kinetic studies indicated that the ligand-controlled regiodivergent reactions proceed with a different rate-limiting step, which is consistent with the computational results.

Based on the experimental results and DFT calculations, as well as literature reports,[17b,20] two plausible catalytic pathways

https://doi.org/10.1021/acscatal.4c01312
ACS Catal. 2024, 14, 8505−8517

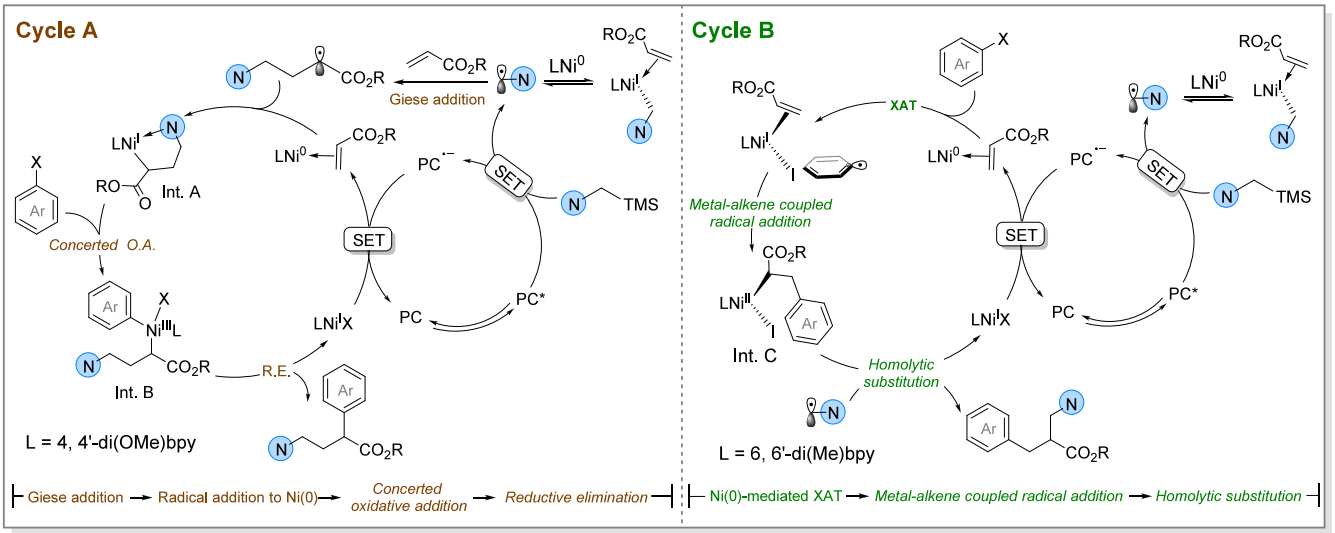

Figure 6. Proposed mechanism.

for the ligand-tuned regiodivergent transformation were shown below (Figure 6). As illustrated in cycle A for the 1,2-aminoalkylarylation process, single electron reduction of α-silylamine ($E_{1/2}^{ox}$ = +0.4−+0.8 V vs SCE)[21] by the excited state of photocatalyst ($E_{1/2}^{PC*/PC^-}$ = +1.35 V vs SCE)[22] generates an α-amino radical, which undergoes Giese addition to alkene to get an α-carbonyl radical, subsequently intercepted by Ni(0) to form Ni(I) intermediate (Int. A) followed by concerted oxidative addition with aryl halides (Int. B) and reductive elimination to afford the 1,2-aminoalkylarylation product. Final single-electron transfer (SET) between Ni(I) [$E_{red}(Ni^I/Ni^0)$ = −1.17 V vs SCE][23] and the reduced state of the photocatalyst ($E_{1/2}^{PC/PC^-}$ = −1.21 V vs SCE)[22] regenerates both catalysts. The competing halogen atom transfer (XAT) pathway for the reaction of aryl halide with the Ni(0) complex is suppressed when employing the bpy ligand possessing a strong coordination ability. Meanwhile, *ortho*-substituted bpy ligand weakens the coordination affinity of alkene to Ni(0) center, thus enhancing the reactivity of XAT to generate aryl radical to trigger the 1,2-arylaminoalkylation process (cycle B). As a consequence, the reaction is preferentially initiated by the metal-alkene coupled radical addition of the aryl radical to generate a triplet alkyl Ni(II) (Int. C) followed by homolytic substitution with α-amino radical that affords the 1,2-arylaminoalkylation product, thus exhibiting an opposite regioselectivity to that in cycle A. In this case, the reaction triggered by the Giese addition with α-amino radical is less favored.

CONCLUSIONS

In conclusion, an unconventional regioreversed 1,2-arylaminoalkylation of electron-deficient alkenes via nickel/photoredox catalysis is developed. This conjugate cross-coupling reaction provides a complementary regioselectivity to our previously reported 1,2-aminoalkylarylation process. Ligands showcase a significant effect on the regiodetermination. Mechanistic experiments provided evidence to support the generation of aryl radical species in this regioreversed process. DFT calculations revealed that the 1,2-aminoalkylarylation process is initiated via Giese addition of α-amino radicals to alkenes followed by radical rebounding to Ni(0), concerted oxidative addition with aryl electrophiles, and C−C reductive elimination. Meanwhile, the 1,2-arylaminoalkylation process is initiated by Ni(0)-mediated XAT, metal-alkene coupled radical addition of aryl radical, and homolytic substitution with α-amino radical. The ligand effects on the regioselectivity are controlled by the reactivity of alkene-coordinated Ni(0)/Ln complex in XAT. Because the higher reactivity in XAT can accelerate the formation of aryl radical, it thus favors the addition of aryl radical to alkene, instead of the α-amino radical addition to alkene. The merger of computational and experimental studies confirmed that both the electronic and steric effects of ligands are crucial for the XAT energy barriers. The delicate variation in the substituents of bpy ligands can alter the regioselectivity by switching the reaction mechanism. We anticipate that these interesting findings will stimulate more endeavors in developing ligand-tuned regiodivergent synthesis via the regulation of reaction pathways.

ASSOCIATED CONTENT

Supporting Information

The Supporting Information is available free of charge at https://pubs.acs.org/doi/10.1021/acscatal.4c01312.

Experimental procedures, characterization data, and ^1H and ^{13}C NMR spectra (PDF)

Computational details (PDF)

X-ray crystallographic information for compound **31** (CIF)

X-ray crystallographic information for compound **52** (CIF)

AUTHOR INFORMATION

Corresponding Authors

Xiaotian Qi − *State Key Laboratory of Power Grid Environmental Protection, College of Chemistry and Molecular Sciences, Wuhan University, Wuhan, Hubei 430072, P. R. China;* orcid.org/0000-0001-5420-5958; Email: qi7xiaotian@whu.edu.cn

Weiming Yuan − *Key Laboratory of Material Chemistry for Energy Conversion and Storage, Ministry of Education, Hubei Key Laboratory of Bioinorganic Chemistry and Materia Medica, School of Chemistry and Chemical Engineering, Huazhong University of Science and Technology (HUST),*

https://doi.org/10.1021/acscatal.4c01312
ACS Catal. 2024, 14, 8505−8517

Wuhan 430074, P.R. China; Shenzhen Huazhong University of Science and Technology Research Institute, Shenzhen 518000, P. R. China; orcid.org/0000-0002-0766-960X; Email: yuanwm@hust.edu.cn

Authors

Fu Ye − *Key Laboratory of Material Chemistry for Energy Conversion and Storage, Ministry of Education, Hubei Key Laboratory of Bioinorganic Chemistry and Materia Medica, School of Chemistry and Chemical Engineering, Huazhong University of Science and Technology (HUST), Wuhan 430074, P.R. China*

Songlin Zheng − *Hubei Three Gorges Laboratory, Yichang 443007, P. R. China*

Yixin Luo − *State Key Laboratory of Power Grid Environmental Protection, College of Chemistry and Molecular Sciences, Wuhan University, Wuhan, Hubei 430072, P. R. China; State Key Laboratory of Antiviral Drugs, Pingyuan Laboratory, Henan Normal University, Xinxiang, Henan 453007, P. R. China*

Complete contact information is available at: https://pubs.acs.org/10.1021/acscatal.4c01312

Author Contributions

#F.Y., S.Z., and Y.L. contributed equally.

Notes

The authors declare no competing financial interest.

■ ACKNOWLEDGMENTS

W.Y. acknowledges the financial support from the National Natural Science Foundation of China (22201087) and the Guangdong Basic and Applied Basic Research Foundation (2022A1515012507). X.Q. acknowledges the financial support from the National Natural Science Foundation of China (22201222), the National Key R&D Program of China (2022YFA1505100), the Fundamental Research Funds for the Central Universities (2042022kf1041), and the supercomputing system in the Supercomputing Center of Wuhan University. We thank Prof. Mian Guo and Dr. Qinghong Yang at Wuhan University for their help in UV−vis and EPR experiments.

■ REFERENCES

(1) For recent reviews, see: (a) Derosa, J.; Apolinar, O.; Kang, T.; Tran, V. T.; Engle, K. M. Recent Developments in Nickel-catalyzed Intermolecular Dicarbofunctionalization of Alkenes. *Chem. Sci.* **2020**, *11*, 4287−4296. (b) Giri, R.; Ks, S. Strategies toward Dicarbofunctionalization of Unactivated Olefins by Combined Heck Carbometalation and Cross-Coupling. *J. Org. Chem.* **2018**, *83*, 3013−3022. (c) Qi, X.; Diao, T. Nickel-Catalyzed Dicarbofunctionalization of Alkenes. *ACS Catal.* **2020**, *10*, 8542−8556. (d) Diccianni, J.; Lin, Q.; Diao, T. Mechanisms of Nickel-Catalyzed Coupling Reactions and Applications in Alkene Functionalization. *Acc. Chem. Res.* **2020**, *53*, 906−919. (e) Zhu, S.-Q.; Zhao, X.; Li, H.; Chu, L. Catalytic three-component dicarbofunctionalization reactions involving radical capture by nickel. *Chem. Soc. Rev.* **2021**, *50*, 10836−10856.

(2) (a) Derosa, J.; Tran, V. T.; Boulous, M. N.; Chen, J. S.; Engle, K. M. Nickel-Catalyzed *β,γ*-Dicarbofunctionalization of Alkenyl Carbonyl Compounds via Conjunctive Cross-Coupling. *J. Am. Chem. Soc.* **2017**, *139*, 10657−10660. (b) Derosa, J.; Kleinmans, R.; Tran, V. T.; Karunananda, M. K.; Wisniewski, S. R.; Eastgate, M. D.; Engle, K. M. Nickel-Catalyzed 1,2-Diarylation of Simple Alkenyl Amides. *J. Am. Chem. Soc.* **2018**, *140*, 17878−17883. (c) Shrestha, B.; Basnet, P.; Dhungana, R. K.; Kc, S.; Thapa, S.; Sears, J. M.; Giri, R. Ni-Catalyzed Regioselective 1,2-Dicarbofunctionalization of Olefins by Intercepting Heck Intermediates as Imine-Stabilized Transient Metallacycles. *J. Am. Chem. Soc.* **2017**, *139*, 10653−10656. (d) Basnet, P.; Kc, S.; Dhungana, R. K.; Shrestha, B.; Boyle, T. J.; Giri, R. Synergistic Bimetallic Ni/Ag and Ni/Cu Catalysis for Regioselective *γ,δ*-Diarylation of Alkenyl Ketimines: Addressing *β*-H Elimination by in Situ Generation of Cationic Ni(II) Catalysts. *J. Am. Chem. Soc.* **2018**, *140*, 15586−15590. (e) Li, W.; Boon, J. K.; Zhao, Y. Nickel-catalyzed Difunctionalization of Allyl Moieties Using Organoboronic Acids and Halides with Divergent Regioselectivities. *Chem. Sci.* **2018**, *9*, 600−607. (f) Gao, P.; Chen, L.-A.; Brown, M. K. Nickel-Catalyzed Stereoselective Diarylation of Alkenylarenes. *J. Am. Chem. Soc.* **2018**, *140*, 10653−10657.

(3) For recent publications, see: (a) Qin, T.; Cornella, J.; Li, C.; Malins, L. R.; Edwards, J. T.; Kawamura, S.; Maxwell, B. D.; Eastgate, M. D.; Baran, P. S. A General Alkyl-alkyl Cross-coupling Enabled by Redox-active Esters and Alkylzinc Reagents. *Science* **2016**, *352*, 801−805. (b) Gu, J.-W.; Min, Q.-Q.; Yu, L.-C.; Zhang, X. Tandem Difluoroalkylation-Arylation of Enamides Catalyzed by Nickel. *Angew. Chem., Int. Ed.* **2016**, *55*, 12270−12274. (c) Kc, S.; Dhungana, R. K.; Shrestha, B.; Thapa, S.; Khanal, N.; Basnet, P.; Lebrun, R. W.; Giri, R. Ni-Catalyzed Regioselective Alkylarylation of Vinylarenes via $C(sp^3)$−$C(sp^3)$/$C(sp^3)$−$C(sp^2)$ Bond Formation and Mechanistic Studies. *J. Am. Chem. Soc.* **2018**, *140*, 9801−9805. (d) Dhungana, R. K.; Sapkota, R. R.; Wickham, L. M.; Niroula, D.; Giri, R. Ni-Catalyzed Regioselective 1,2-Dialkylation of Alkenes Enabled by the Formation of Two $C(sp^3)$−$C(sp^3)$ Bonds. *J. Am. Chem. Soc.* **2020**, *142*, 20930−20936. (e) Derosa, J.; van der Puyl, V. A.; Tran, V. T.; Liu, M.; Engle, K. M. Directed Nickel-catalyzed 1,2-Dialkylation of Alkenyl Carbonyl Compounds. *Chem. Sci.* **2018**, *9*, 5278−5283. (f) Chierchia, M.; Xu, P.; Lovinger, G. J.; Morken, J. P. Enantioselective Radical Addition/Cross-Coupling of Organozinc Reagents, Alkyl Iodides, and Alkenyl Boron Reagents. *Angew. Chem., Int. Ed.* **2019**, *58*, 14245−14249. (g) García-Domínguez, A.; Li, Z.; Nevado, C. Nickel-Catalyzed Reductive Dicarbofunctionalization of Alkenes. *J. Am. Chem. Soc.* **2017**, *139*, 6835−6838. (h) Shu, W.; García-Domínguez, A.; Quirós, M. T.; Mondal, R.; Cárdenas, D. J.; Nevado, C. Ni-Catalyzed Reductive Dicarbofunctionalization of Nonactivated Alkenes: Scope and Mechanistic Insights. *J. Am. Chem. Soc.* **2019**, *141*, 13812−13821. (i) Zhao, X.; Tu, H.-Y.; Guo, L.; Zhu, S.; Qing, F.-L.; Chu, L. Intermolecular Selective Carboacylation of Alkenes via Nickel-catalyzed Reductive Radical Relay. *Nat. Commun.* **2018**, *9*, 3488−3494. (j) Yang, T.; Jiang, Y.; Luo, Y.; Lim, J. J. H.; Lan, Y.; Koh, M. J. Chemoselective Union of Olefins, Organohalides, and Redox-Active Esters Enables Regioselective Alkene Dialkylation. *J. Am. Chem. Soc.* **2020**, *142*, 21410−21419. (k) Wang, X.-X.; Lu, X.; He, S.-J.; Fu, Y. Nickel-catalyzed Three-component Olefin Reductive Dicarbofunctionalization to Access Alkylborates. *Chem. Sci.* **2020**, *11*, 7950−7956. (l) Wei, X.; Shu, W.; García-Domínguez, A.; Merino, E.; Nevado, C. Asymmetric Ni-Catalyzed Radical Relayed Reductive Coupling. *J. Am. Chem. Soc.* **2020**, *142*, 13515−13522. (m) Tu, H.-Y.; Wang, F.; Huo, L.; Li, Y.; Zhu, S.; Zhao, X.; Li, H.; Qing, F.-L.; Chu, L. Enantioselective Three-Component Fluoroalkylarylation of Unactivated Olefins through Nickel-Catalyzed Cross-Electrophile Coupling. *J. Am. Chem. Soc.* **2020**, *142*, 9604−9611.

(4) For selected reviews on metallaphotoredox catalysis, see: (a) Chan, A. Y.; Perry, I. B.; Bissonnette, N. B.; Buksh, B. F.; Edwards, G. A.; Frye, L. I.; Garry, O. L.; Lavagnino, M. N.; Li, B. X.; Liang, Y.; Mao, E.; Millet, A.; Oakley, J. V.; Reed, N. L.; Sakai, H. A.; Seath, C. P.; MacMillan, D. W. C. Metallaphotoredox: The Merger of Photoredox and Transition Metal Catalysis. *Chem. Rev.* **2022**, *122*, 1485−1542. (b) Tellis, J. C.; Kelly, C. B.; Primer, D. N.; Jouffroy, M.; Patel, N. R.; Molander, G. A. Single-Electron Transmetalation via Photoredox/Nickel Dual Catalysis: Unlocking a New Paradigm for sp^3−sp^2 Cross-Coupling. *Acc. Chem. Res.* **2016**, *49*, 1429−1439.

(5) (a) Guo, L.; Tu, H.-Y.; Zhu, S.; Chu, L. Selective, Intermolecular Alkylarylation of Alkenes via Photoredox/Nickel Dual Catalysis. *Org. Lett.* **2019**, *21*, 4771−4776. (b) García-Domínguez, A.; Mondal, R.; Nevado, C. Dual Photoredox/Nickel-Catalyzed Three-Component

Carbofunctionalization of Alkenes. *Angew. Chem., Int. Ed.* **2019**, *58*, 12286−12290. (c) Campbell, M. W.; Compton, J. S.; Kelly, C. B.; Molander, G. A. Three-Component Olefin Dicarbofunctionalization Enabled by Nickel/Photoredox Dual Catalysis. *J. Am. Chem. Soc.* **2019**, *141*, 20069−20078. (d) Guo, L.; Yuan, M.; Zhang, Y.; Wang, F.; Zhu, S.; Gutierrez, O.; Chu, L. General Method for Enantioselective Three-Component Carboarylation of Alkenes Enabled by Visible-Light Dual Photoredox/Nickel Catalysis. *J. Am. Chem. Soc.* **2020**, *142*, 20390−20399. (e) Mega, R. S.; Duong, V. K.; Noble, A.; Aggarwal, V. K. Decarboxylative Conjunctive Cross-coupling of Vinyl Boronic Esters using Metallaphotoredox Catalysis. *Angew. Chem., Int. Ed.* **2020**, *59*, 4375−4379. (f) Campbell, M. W.; Yuan, M.; Polites, V. C.; Gutierrez, O.; Molander, G. A. Photochemical C−H Activation Enables Nickel-Catalyzed Olefin Dicarbofunctionalization. *J. Am. Chem. Soc.* **2021**, *143*, 3901−3910. (g) Xu, S.; Chen, H.; Zhou, Z.; Kong, W. Three-Component Alkene Difunctionalization by Direct and Selective Activation of Aliphatic C−H Bonds. *Angew. Chem., Int. Ed.* **2021**, *60*, 7405−7411. (h) Sun, S.-Z.; Duan, Y.; Mega, R. S.; Somerville, R. J.; Martin, R. Site-Selective 1,2-Dicarbofunctionalization of Vinyl Boronates through Dual Catalysis. *Angew. Chem., Int. Ed.* **2020**, *59*, 4370−4374. (i) Qian, P.; Guan, H.; Wang, Y.-E.; Lu, Q.; Zhang, F.; Xiong, D.; Walsh, P. J.; Mao, J. Catalytic enantioselective reductive domino alkyl arylation of acrylates via nickel/photoredox catalysis. *Nat. Commun.* **2021**, *12*, 6613−6621.

(6) For reviews, see: (a) Zhu, C.; Yue, H.; Chu, L.; Rueping, M. Recent Advances in Photoredox and Nickel Dual-catalyzed Cascade Reactions: Pushing the Boundaries of Complexity. *Chem. Sci.* **2020**, *11*, 4051−4064. (b) Badir, S. O.; Molander, G. A. Developments in Photoredox/Nickel Dual-Catalyzed 1,2-Difunctionalizations. *Chem.* **2020**, *6*, 1327−1339.

(7) Parsaee, F.; Senarathna, M. C.; Kannangara, P. B.; Alexander, S. N.; Arche, P. D. E.; Welin, E. R. Radical philicity and its role in selective organic transformations. *Nat. Chem. Rev.* **2021**, *5*, 486−499.

(8) (a) Giese, B. Formation of CC Bonds by Addition of Free Radicals to Alkenes. *Angew. Chem., Int. Ed.* **1983**, *22*, 753−764. (b) Fischer, H.; Radom, L. Factors Controlling the Addition of Carbon-Centered Radicals to Alkenes−An Experimental and Theoretical Perspective. *Angew. Chem., Int. Ed.* **2001**, *40*, 1340−1371.

(9) Zheng, S.; Chen, Z.; Hu, Y.; Xi, X.; Liao, Z.; Li, W.; Yuan, W. Selective 1,2-Aryl-Aminoalkylation of Alkenes Enabled by Metallaphotoredox Catalysis. *Angew. Chem., Int. Ed.* **2020**, *59*, 17910−17916.

(10) (a) Zheng, S.; Wang, W.; Yuan, W. Remote and Proximal Hydroaminoalkylation of Alkenes Enabled by Photoredox/Nickel Dual Catalysis. *J. Am. Chem. Soc.* **2022**, *144*, 17776−17782. (b) Ye, F.; Yang, Y.; Wang, W.; Yuan, W. Nickel and photoredox dual-catalyzed regioselective dialkylation of alkenes. *Chem. Catal.* **2023**, *3*, 100605. (c) Zhao, H.; Yuan, W. Three-component reductive conjugate addition/aldol tandem reaction enabled by nickel/photoredox dual catalysis. *Chem. Sci.* **2023**, *14*, 1485−1490. (d) Xi, X.; Chen, Y.; Yuan, W. Nickel-Catalyzed Three-Component Alkylacylation of Alkenes Enabled by a Photoactive Electron Donor−Acceptor Complex. *Org. Lett.* **2022**, *24*, 3938−3943.

(11) (a) Nájera, C.; Beletskaya, I. P.; Yus, M. Metal-catalyzed regiodivergent organic reactions. *Chem. Soc. Rev.* **2019**, *48*, 4515−4618. (b) Li, Y.; Wu, D.; Cheng, H.-G.; Yin, G. Difunctionalization of Alkenes Involving Metal Migration. *Angew. Chem., Int. Ed.* **2020**, *59*, 7990−8003. (c) Belal, M.; Li, Z.; Zhu, L.; Yin, G. Catalyst-controlled regiodivergent 1,2-difunctionalization of alkenes with two carbon-based electrophiles. *Sci. China. Chem.* **2022**, *65*, 514−520.

(12) (a) Cabrele, C.; Martinek, T. A.; Reiser, O.; Berlicki, L. Peptides Containing *β*-Amino Acid Patterns: Challenges and Successes in Medicinal Chemistry. *J. Med. Chem.* **2014**, *57*, 9718−9739. (b) Kudo, F.; Miyanaga, A.; Eguchi, T. Biosynthesis of natural products containing *β*-amino acids. *Nat. Prod. Rep.* **2014**, *31*, 1056−1073.

(13) Masako, H.; Sachiko, M.; Hiroshi, N.; Hiroki, K.; Yukari, M. Alpha Aryl or Heteroaryl Methyl Beta Piperidine Propanamide Compounds as ORL1-receptor Antagonist. PCT Int. Appl. WO 2005/092858 A2.

(14) (a) Desnoyer, A. N.; He, W.; Behyan, S.; Chiu, W.; Love, J. A.; Kennepohl, P. The Importance of Ligand-induced Backdonation in the Stabilization of Square Planar d^{10} Nickel *π*-Complexes. *Chem.—Eur. J.* **2019**, *25*, 5259−5268. (b) Nattmann, L.; Saeb, R.; Nöthling, N.; Cornella, J. An air-stable binary Ni(0)−olefin catalyst. *Nat. Catal.* **2020**, *3*, 6−13.

(15) (a) Funes-Ardoiz, I.; Nelson, D. J.; Maseras, F. Halide Abstraction Competes with Oxidative Addition in the Reactions of Aryl Halides with $[Ni(PMe_nPh_{(3-n)})_4]$. *Chem.—Eur. J.* **2017**, *23*, 16728−16733. (b) Juliá, F.; Constantin, T.; Leonori, D. Applications of halogen-atom transfer (XAT) for the generation of carbon radicals in synthetic photochemistry and photocatalysis. *Chem. Rev.* **2022**, *122*, 2292−2352. (c) de Aguirre, A.; Funes-Ardoiz, I.; Maseras, F. Four Oxidation States in a Single Photoredox Nickel-Based Catalytic Cycle: A Computational Study. *Angew. Chem., Int. Ed.* **2019**, *58*, 3898−3902.

(16) (a) Boyington, A. J.; Seath, C. P.; Zearfoss, A. M.; Xu, Z.; Jui, N. T. Catalytic Strategy for Regioselective Arylethylamine Synthesis. *J. Am. Chem. Soc.* **2019**, *141*, 4147−4153. (b) Le, C.; Chen, T. Q.; Liang, T.; Zhang, P.; MacMillan, D. W. C. A radical approach to the copper oxidative addition problem: Trifluoromethylation of bromoarenes. *Science* **2018**, *360*, 1010−1014. (c) Kindt, S.; Heinrich, M. R. Recent Advances in Meerwein Arylation Chemistry. *Synthesis* **2016**, *48*, 1597−1606.

(17) (a) Matsui, J. K.; Gutiérrez-Bonet, Á.; Rotella, M.; Alam, R.; Gutierrez, O.; Molander, G. A. Photoredox/Nickel-Catalyzed Single-Electron Tsuji−Trost Reaction: Development and Mechanistic Insights. *Angew. Chem., Int. Ed.* **2018**, *57*, 15847−15851. (b) Yuan, M.; Song, Z.; Badir, S. O.; Molander, G. A.; Gutierrez, O. On the Nature of $C(sp^3)-C(sp^2)$ Bond Formation in Nickel-Catalyzed Tertiary Radical Cross-Couplings: A Case Study of Ni/Photoredox Catalytic Cross-Coupling of Alkyl Radicals and Aryl Halides. *J. Am. Chem. Soc.* **2020**, *142*, 7225−7234.

(18) Shen, Y.; Rovis, T. Late-Stage N-Me Selective Arylation of Trialkylamines Enabled by Ni/Photoredox Dual Catalysis. *J. Am. Chem. Soc.* **2021**, *143*, 16364−16369.

(19) Wu, J.-Y.; Mo, B.-R.; Yang, J.-D.; Cheng, J.-P. A Distinctive Pattern for Substituent Effects on Transition Metal Centers: Enhanced Electron-Donating Capacity of Cationic Palladium Species. *CCS Chem.* **2023**, *5*, 1163−1175.

(20) For mechanistic studies on photoredox/nickel dual-catalyzed cross-couplings, see: (a) Gutierez, O.; Tellis, J. C.; Primer, D. N.; Molander, G. A.; Kozlowski, M. C. Nickel-Catalyzed Cross-Coupling of Photoredox-Generated Radicals: Uncovering a General Manifold for Stereoconvergence in Nickel-Catalyzed Cross-Couplings. *J. Am. Chem. Soc.* **2015**, *137*, 4896−4899. (b) Xi, X.; Luo, Y.; Li, W.; Xu, M.; Zhao, H.; Chen, Y.; Zheng, S.; Qi, X.; Yuan, W. From Esters to Ketones via a Photoredox-Assisted Reductive Acyl Cross-Coupling Strategy. *Angew. Chem., Int. Ed.* **2022**, *61*, e202114731.

(21) Yoshida, J.; Maekawa, T.; Murata, T.; Matsunaga, S.; Isoe, S. Electrochemical oxidation of organosilicon compounds. Part 7. The origin of. beta. -silicon effect in electron-transfer reactions of silicon-substituted heteroatom compounds. Electrochemical and theoretical studies. *J. Am. Chem. Soc.* **1990**, *112*, 1962−1970.

(22) Luo, J.; Zhang, J. Donor-Acceptor Fluorophores for Visible-Light-Promoted Organic Synthesis: Photoredox/Ni Dual Catalytic $C(sp^3)-C(sp^2)$ Cross-Coupling. *ACS Catal.* **2016**, *6*, 873−877.

(23) Shields, B. J.; Doyle, A. G. Direct $C(sp^3)$−H Cross Coupling Enabled by Catalytic Generation of Chlorine Radicals. *J. Am. Chem. Soc.* **2016**, *138*, 12719−12722.

https://doi.org/10.1021/acscatal.4c01312
ACS Catal. 2024, 14, 8505−8517